

## Supplementary Online Material

# **Cryo-EM Structure of the Archaeal 50S Ribosomal Subunit in Complex with Initiation Factor 6 and Implications for Ribosome Evolution**

Basil J. Greber, Daniel Boehringer, Vlatka Godinic-Mikulcic, Ana Crnkovic, Michael Ibba,  
Ivana Weygand-Durasevic, Nenad Ban<sup>\*</sup>

<sup>\*</sup> To whom correspondence should be addressed. E-mail: ban@mol.biol.ethz.ch, phone:  
+41 44 633 27 85, fax: +41 44 633 12 46.

## Supplementary Text

### Analysis of Conserved Residues in IF6

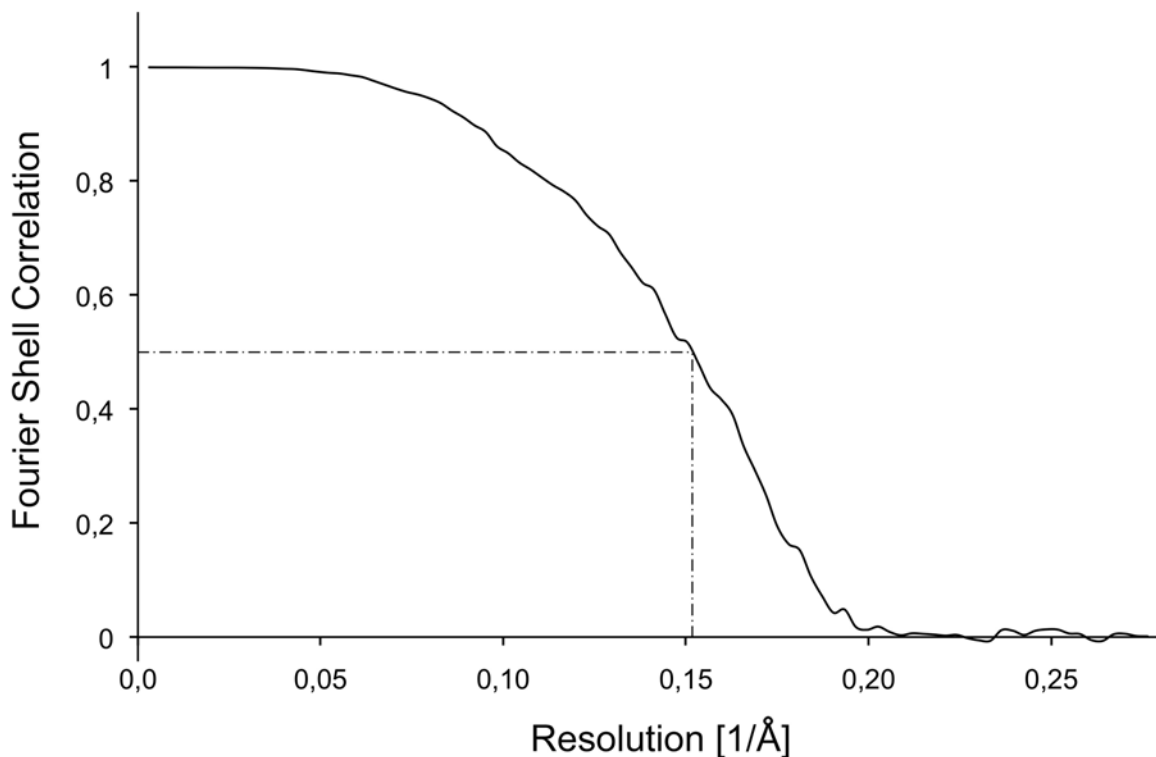
The most highly conserved residues in IF6 do not cluster on the ribosome binding surface of IF6 and are mostly buried (Fig. S3b), suggesting that most of them are required for IF6 stability and folding rather than making ribosome binding. Based on genetic studies in yeast, the mutation of several of these conserved residues has been reported to reduce the stability of eIF6 binding to the large ribosomal subunit<sup>1</sup>. This includes the residues corresponding to the universally conserved Gly14, Gly105 and Asn106 (*S. cerevisiae* numbering<sup>1</sup>). The glycines are located on the inward facing side of the ring of helical segments that forms part of the ribosome interacting surface of IF6 (Fig. S3b). Mutations in these residues may structurally distort IF6 in a way that reduces the interactions of nearby residues with the ribosomal subunit. Asn106, in contrast, is located on the surface of IF6 and contacts the ribosome. In addition to these highly conserved residues, several less strictly conserved residues found on the ribosome binding face of IF6 are also affected by mutations that weaken the interaction between the ribosomal subunit and IF6<sup>1</sup>.

### Possible Causes for the Loss of Ribosomal Proteins in Euryarchaeota

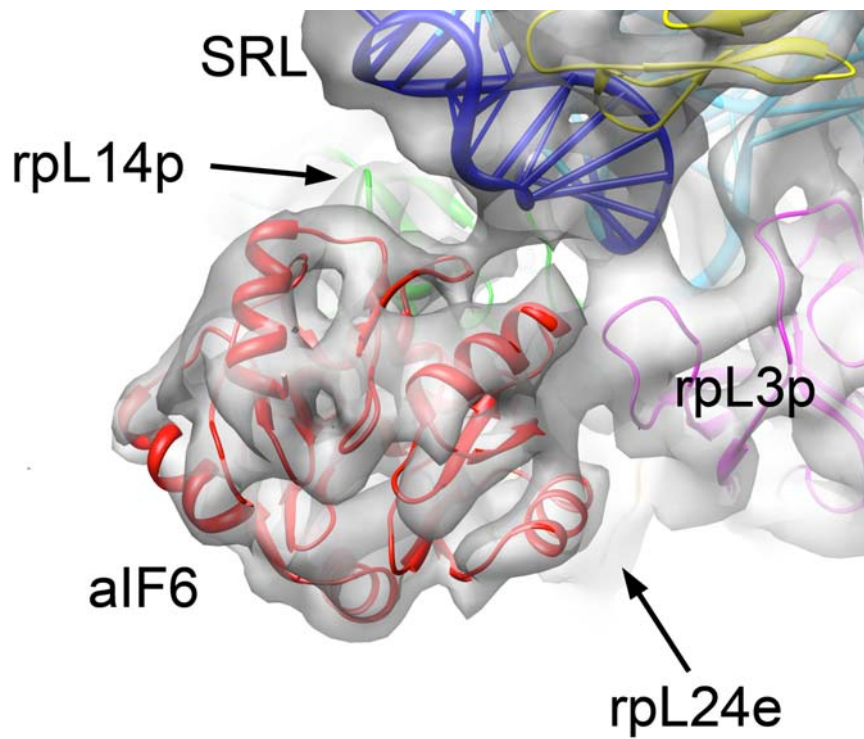
In archaea, the distribution of ribosomal proteins exhibits a domain wide trend towards a more and more reduced ribosomal proteome in late branching *Euryarchaeota*<sup>2</sup>. Some cases of ribosomal protein loss in bacteria and eukaryotes have been observed in organisms that have undergone genome reduction<sup>2</sup>. Genome reduction is mostly associated with specific lifestyles of the affected organisms as obligate pathogens<sup>3; 4; 5; 6</sup>, endosymbionts<sup>7</sup>, or obligate parasites<sup>8</sup>, but has also been reported for free living mesophilic bacteria<sup>9; 10</sup>. However, the reduction of the ribosomal proteome in *Euryarchaeota* does not seem to correlate with genome size (preliminary analysis, data not shown), suggesting that the reduction of the ribosomal proteome is not caused by genome compaction. This does not exclude the possibility that genome compaction is responsible for the loss of ribosomal proteins in some species, but suggests that it may not be the cause of the domain-wide trend<sup>2</sup> of ribosomal protein loss in archaea.

Possibly, ribosome assembly or function is influenced by the physico-chemical intracellular conditions and growth regimes associated with the extreme lifestyles of many archaea, contributing to the observed decline in the number of ribosomal proteins throughout euryarchaeota. Some ribosomal proteins might no longer be required in some environments, or evolution of a more compact, more stable ribosomal particle might confer some selective advantages. Additionally, the constraints imposed on the amino acid composition and structure of proteins in extreme environments, such as acidification of the proteome in halophiles, may be a contributing factor<sup>11; 12; 13</sup>.

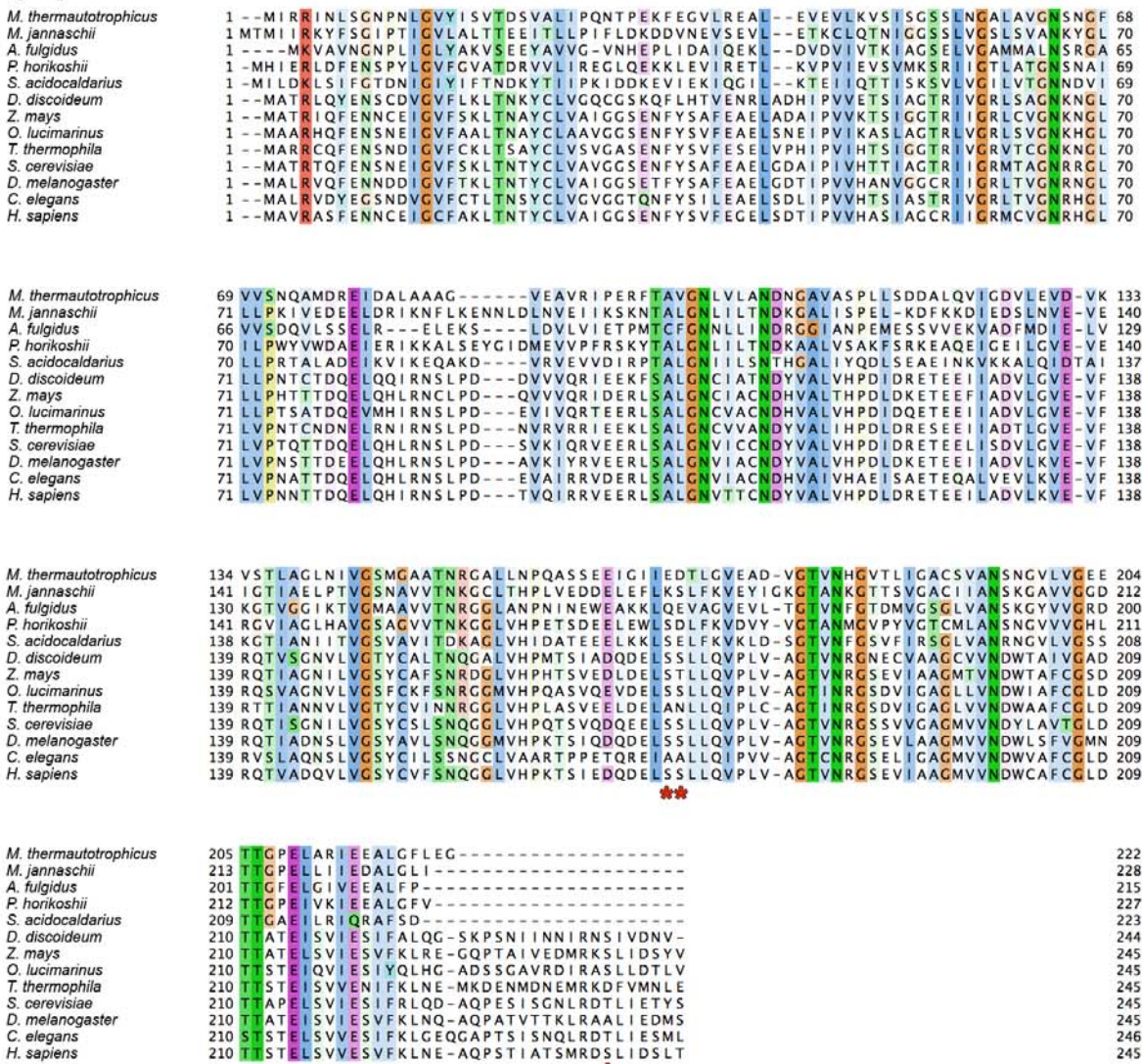
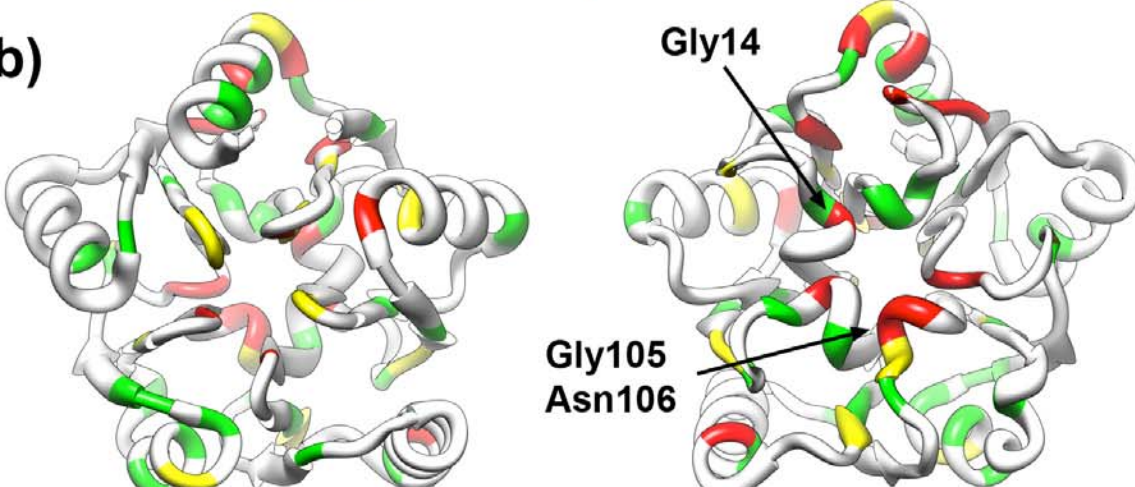
## Supplementary Figures



**Fig. S1.** Fourier Shell Correlation (FSC) curve of the final contoured 50S-aIF6 cryo-EM map calculated from masked density maps. The resolution estimate is 6.6 Å at FSC = 0.5 and 5.5 Å at FSC = 0.143<sup>14</sup>. Based on the features observed in the cryo-EM map, the FSC = 0.5 criterion is applied for its interpretation throughout the manuscript.



**Fig. S2.** Additional view of the binding site of aIF6 on the 50S ribosomal subunit (rotated from Fig. 3c). The Sarcin-Ricin-Loop is depicted in deep blue, aIF6 in red, rpL14p in green, rpL3p in magenta, and rpL24e in orange.

**(a)****(b)**

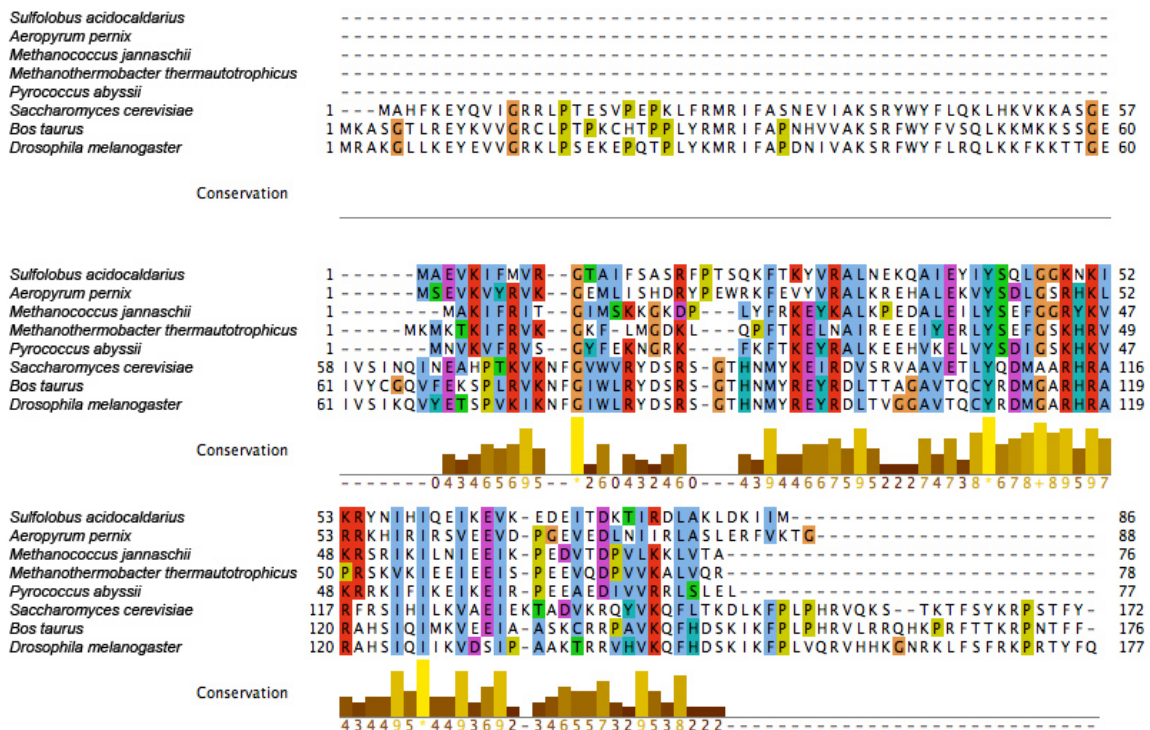
**Fig. S3.** (a) Multiple sequence alignment of IF6 protein sequences from selected eukaryotic and archaeal organisms. The incompletely conserved phosphorylatable Serine residues 174, 175, and 235<sup>15; 16; 17</sup> are marked with red asterisks. Phosphorylation of Ser235 is controversial

<sup>17; 18</sup>. (b) Ribbon diagrams of the *M. jannaschii* aIF6 X-ray crystal structure (PDB ID: **1G61** <sup>19</sup>) (left: solvent side; right: ribosome interaction surface) colored according to Clustal characters (red: identity according to (a); green, yellow, white: conservation in descending order). The highly conserved Gly14, Gly105, and Asn106 (*S. cerevisiae* nomenclature) are discussed in the supplementary text (see above).



**Fig. S4.** Aligned 23S rRNA sequences of *M. thermautotrophicus* (*Mt*) and *H. marismortui* (*Hm*) extracted from a multiple sequence alignment of archaeal 23S rRNA<sup>20</sup> (Comparative RNA Website, <http://www.rna.ccbb.utexas.edu>). 23S rRNA expansions in *M. thermautotrophicus* are indicated, and labelled with the designation of the corresponding eukaryotic rRNA sequence element. A red asterisk next to the segment designation indicates that the corresponding expansion is of sufficient size to be interpreted by docking of a model into the *M. thermautotrophicus* 50S cryo-EM map.

**(a)**



**(b)**

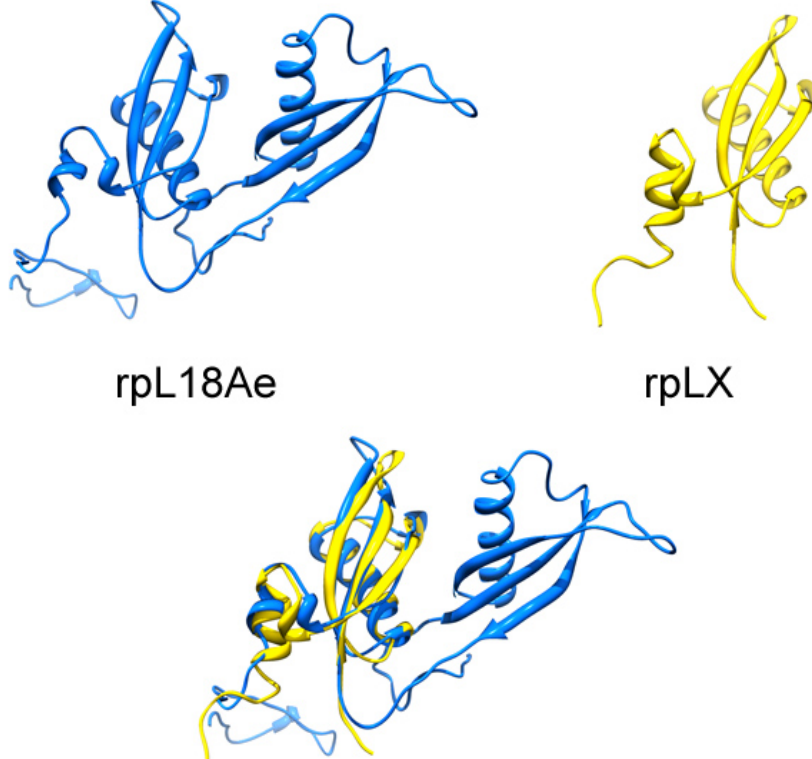


**Fig. S5.** (a) Multiple sequence alignment showing the homology between rpL18Ae (eukaryotes: *S. cerevisiae*, *B. taurus*, *D. melanogaster*) and rpLX (archaea: *S. acidocaldarius*,

*A. pernix*, *M. jannaschii*, *M. thermautotrophicus*, *P. abyssii*). (b) Comparison of the X-ray crystal structure of ribosome-bound rpL18Ae<sup>21</sup> (*T. thermophila*; blue) and the solution structure of rpLX (*M. thermautotrophicus*, PDB ID: **2JXT**; yellow).

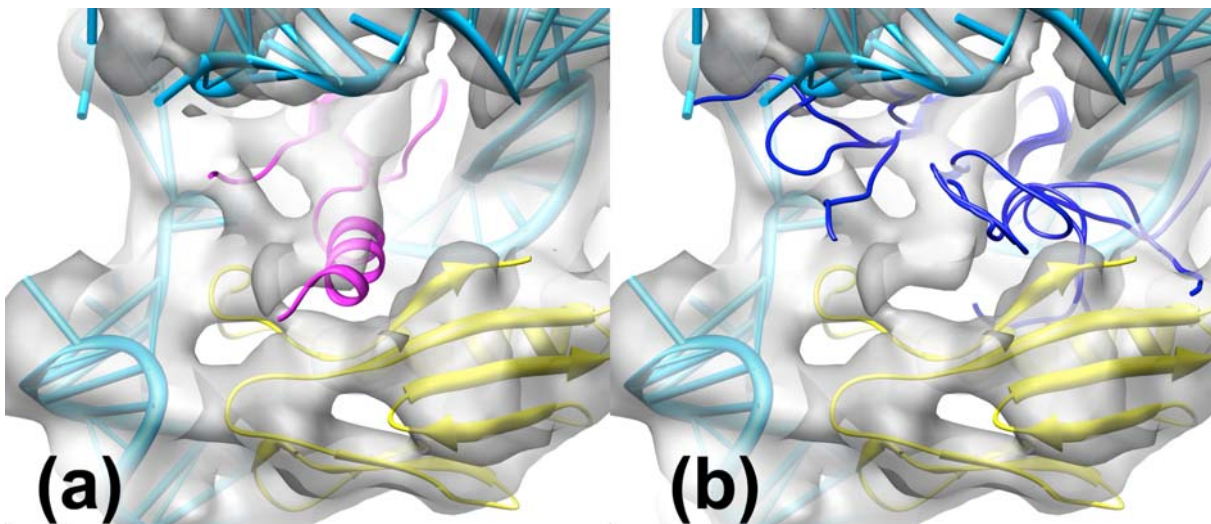


**Fig. S6.** Ribosomal protein rpL40e may fold fully only after making contact with ribosomal RNA. (a) *M. thermautotrophicus* rpL40e (pink) modelled according to the ribosome-bound *T. thermophila* template<sup>21</sup> shown in the 50S-aIF6 density. (b) Solution structure of *S. solfataricus* rpL40e (dark blue; PDB ID: **2AYJ**, chains A-D) aligned onto the *Mt* rpL40e core fold. The density features are consistent with formation of an  $\alpha$ -helix at the rpL40e N-terminus upon binding to the ribosomal subunit. Ribosomal protein rpL6p in pale yellow, 23S rRNA in sky blue.

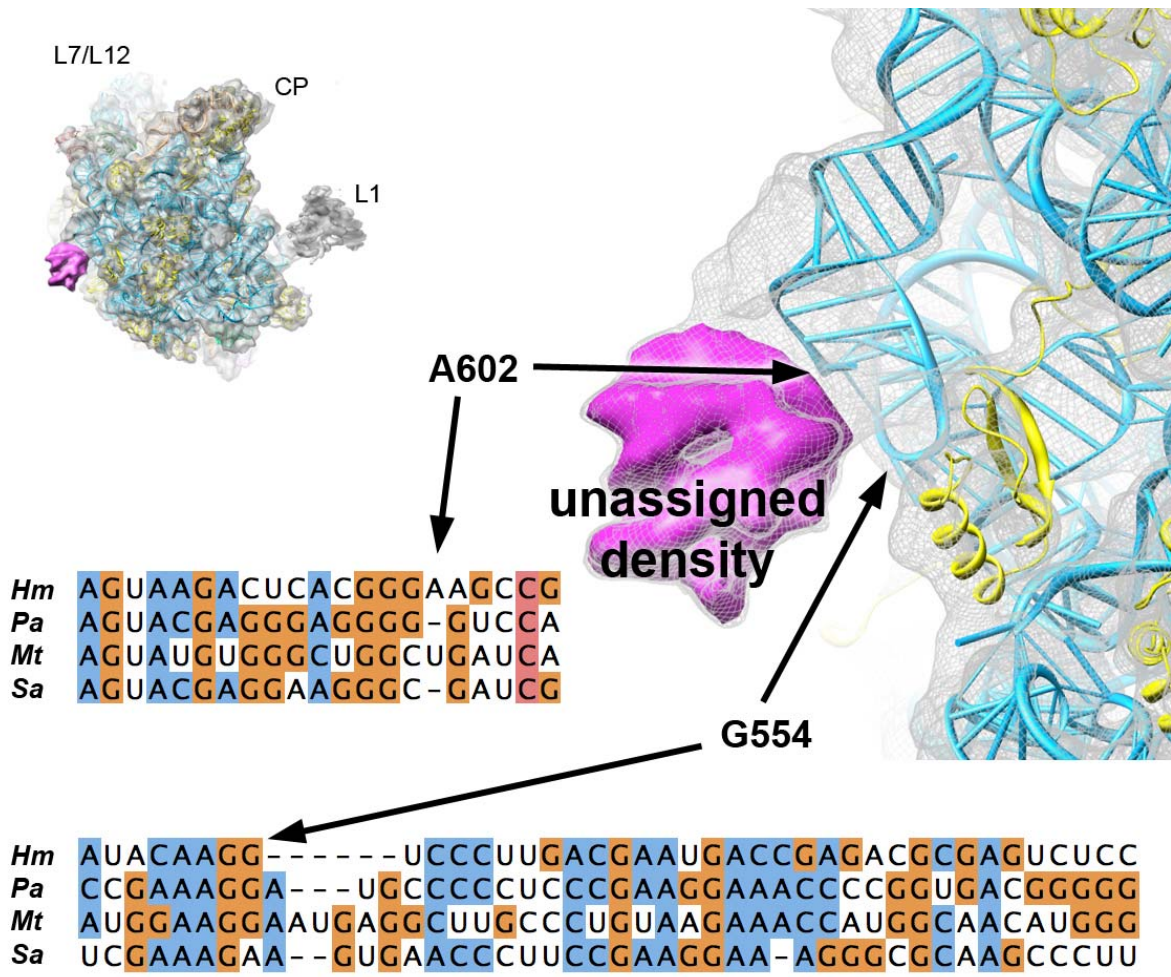


**Fig. S7.** The unassigned density on the solvent side of the *M. thermautotrophicus* 50S subunit corresponds most likely to an unidentified protein. No rRNA expansions of sufficient size are present in the immediate vicinity, and the variability of rRNA in this region does not correlate with the presence of this density in *S. acidocaldarius* (*Sa*) and *M. thermautotrophicus* (*Mt*) and its absence in *P. aerophilum* (*Pa*) and *H. marismortui* (*Hm*). The inset shows the 50S-aIF6 complex in the same orientation as the main figure. The L1 and L7/L12 stalks and the central protuberance (CP) are labeled. The sequence alignment was taken from a multiple sequence alignment of archaeal 23S rRNA<sup>20</sup> (Comparative RNA Website, <http://www.rna.ccb.utexas.edu>). A new alignment of only the four displayed sequences using ClustalX<sup>22</sup> resulted in only minor changes of the alignment (not shown) and did not affect the conclusion. The depiction of the molecular model and the alignment were created in Chimera<sup>23</sup> and JalView 2.4<sup>24</sup>, respectively.

**Table S1.** Overview of the *M. thermautotrophicus* (*Mt*) large ribosomal subunit protein analysis by LC-MS/MS (green: protein found; red: protein not found).

<i>Mt</i> ribosomal protein	Molecular weight (kDa)	LC-MS/MS	<i>Mt</i> ribosomal protein	Molecular weight (kDa)	LC-MS/MS
rpL3P	37.3		rpL18e	13.5	
rpLP0/rpL10P	36.5		rpL7Ae	13.2	
rpL4P	28.3		rpL32e	12.6	
rpL2P	26.1		rpL21e	11.1	
rpL1P	23.8		rpL44e	10.9	
rpL15e	21.9		rpL12P	10.5	
rpL18P	21.6		rpL30e	10.5	
rpL6P	19.8		rpL34e	10.3	red
rpL5P	19.4		rpL23P	9.9	
rpL10e	18.1		rpL37Ae	9.9	red
rpL11p	17.5		rpL31e	9.4	
rpL22P	17.3		rpLX	9.3	
rpL30P	17.1		rpL14e	8.3	
rpL19e	17.1		rpL29P	7.4	
rpL15P	16.5		rpL37e	7.1	red
rpL13P	16.1 <sup>a</sup>		rpL39e	6.4	
rpL14P	14.2		rpL24e	6.3	red
rpL24P	13.9		rpL40e	5.6	

<sup>a</sup> estimate based on alignment of rpL13P/rpS9 fusion protein annotated in

*M. thermautotrophicus* genome with *M. marburgensis* homolog

**Table S2.** Assignment of the rotational orientation of aIF6 on the 50S ribosomal subunit by cross-correlation. The cross-correlation was computed using the fit in map command in Chimera, using a map simulated from the *M. thermautotrophicus* aIF6 homology model at 6.7 Å resolution for docking into the cryo-EM density. The rotational position is measured clockwise relative to the position in the 60S-eIF6 complex<sup>21</sup>.

Position	Rotation	Correlation
1	0°	0.82
2	72°	0.78
3	144°	0.77
4	216°	0.80
5	288°	0.76

**Table S3.** Overview of the *H. marismortui* and *M. thermautotrophicus* large ribosomal subunit protein content (SwissProt database<sup>25</sup>). Proteins that were not present in the *H. marismortui* crystal structure<sup>26</sup> but present in the *H. marismortui* genome are indicated in orange, while proteins absent from the *H. marismortui* genome are indicated in green.

<i>M. thermautotrophicus</i> ribosomal protein	<i>H. marismortui</i> ribosomal protein
rpL4P	rpL4P
rpL22P	rpL22P
rpL3P	rpL3P
rpL24P	rpL24P
rpL2P	rpL2P
rpL14P	rpL14P
rpL15P	rpL15P
rpL18P	rpL18P
rpL1P	rpL1P
rpL23P	rpL23P
rpL24e	rpL24e
rpL30P	rpL30P
rpL5P	rpL5P
rpL6P	rpL6P
rpL12P	rpL12P
rpLX	rpLX
rpL13P	rpL13P
rpL10e	rpL10e
rpL11p	rpL11p
rpL14e	-
rpL15e	rpL15e
rpL18e	rpL18e
rpL19e	rpL19e
rpL21e	rpL21e
rpL29P	rpL29P
rpL30e	-

rpL31e	rpL31e
rpL32e	rpL32e
rpL34e	-
rpL37Ae	rpL37Ae
rpL37e	rpL37e
rpL39e	rpL39e
rpL44e	rpL44e
rpL7Ae	rpL7Ae
rpL40e	rpL40e
rpLP0	rpL10P / rpL10E / rplP0

**Table S4.** Generation of the *M. thermautotrophicus* (*Mt*) 50S-aIF6 protein model based on *H. marismortui* (*Hm*), *T. thermophila* (*Tt*), and *M. jannaschii* (*Mj*) protein structures<sup>19; 21; 26</sup>.

<b><i>Mt</i> ribosomal protein</b>	<b>Template ribosomal protein</b>	<b>Source structure for <i>Mt</i> model</b>	<b>Residues used in <i>Mt</i> model</b>	<b>Full length <i>Mt</i> protein</b>	<b>Chain ID in <i>Mt</i> model</b>
rpL2p	<i>Hm</i> rpL2p	3CC2.A	1-238	1-241	A
rpL3p	<i>Hm</i> rpL3p	3CC2.B	1-338	1-337	B
rpL4p	<i>Hm</i> rpL4p	3CC2.C	1-246	1-254	C
rpL5p	<i>Hm</i> rpL5p	3CC2.D	11-176	1-168	D
rpL6p	<i>Hm</i> rpL6p	3CC2.E	1-173	1-177	E
rpL7Ae	<i>Hm</i> rpL7Ae	3CC2.F	1-120	1-123	F
rpL10e	<i>Hm</i> rpL10e	3CC2.H	8-176	1-160	H
rpL13p	<i>Hm</i> rpL13p	3CC2.J	7-145	1-145 <sup>a</sup>	J
rpL14p	<i>Hm</i> rpL14p	3CC2.K	1-132	1-132	K
rpL15p	<i>Hm</i> rpL15p	3CC2.L	1-145	1-146	L
rpL15e	<i>Hm</i> rpL15e	3CC2.M	4-185	1-182	M
rpL18p	<i>Hm</i> rpL18p	3CC2.N	1-185	1-192	N
rpL18e	<i>Hm</i> rpL18e	3CC2.O	1-116	1-121	O
rpL19e	<i>Hm</i> rpL19e	3CC2.P	2-149	1-148	P
rpL21e	<i>Hm</i> rpL21e	3CC2.Q	1-96	1-96	Q
rpL22p	<i>Hm</i> rpL22p	3CC2.R	1-151	1-153	R
rpL23p	<i>Hm</i> rpL23p	3CC2.S	1-85	1-86	S
rpL24p	<i>Hm</i> rpL24p	3CC2.T	1-117	1-117	T
rpL24e	<i>Hm</i> rpL24e	3CC2.U	4-55	1-53	U
rpL29p	<i>Hm</i> rpL29p	3CC2.V	1-64	1-64	V
rpL30p	<i>Hm</i> rpL30p	3CC2.W	1-154	1-152	W
rpL31e	<i>Hm</i> rpL31e	3CC2.X	7-92	1-81	X
rpL32e	<i>Hm</i> rpL32e	3CC2.Y	125-232	1-108	Y
rpL37Ae	<i>Hm</i> rpL37Ae	3CC2.Z	25-114	1-89	Z
rpL37e	<i>Hm</i> rpL37e	3CC2.1	1-57	1-60	1
rpL39e	<i>Hm</i> rpL39e	3CC2.2	1-50	1-51	2

rpL44e	<i>Hm</i> rpL44e	3CC2.3	1-92	1-92	3
rpLX	<i>Mt</i> rpLX	2JXT.A	1-78	1-78	G
rpL40e	<i>Tt</i> rpL40e	4A19.K	80-129	1-48	5
rpL14e	<i>Tt</i> rpL14e	4A19.F	4-80	1-75	7
rpL30e	<i>Tt</i> rpL30e	4A19.G	8-103	1-98	6
rpL34e	<i>Tt</i> rpL34e	4A19.L	8-97	1-88	4
aIF6	<i>Mj</i> aIF6 <sup>b</sup>	1G61.A	3-227 (+1)	1-222	I

<sup>a</sup> estimate based on alignment of rpL13P/rpS9 fusion protein annotated in

*M. thermautotrophicus* genome with *M. marburgensis* homolog

<sup>b</sup> model contains *M. thermautotrophicus* protein sequence

**Table S5.** Generation of the *M. thermautrophicus* (*Mt*) 50S-aIF6 rRNA model based on *H. marismortui* (*Hm*), *T. thermophila* (*Tt*), and *S. cerevisiae* (*Sc*) rRNA structures<sup>21; 26; 27</sup>.

<b><i>Mt</i> rRNA</b>	<b>Template rRNA</b>	<b>Source structure for <i>Mt</i> model</b>	<b>Residues used in <i>Mt</i> model</b>	<b>Chain ID in <i>Mt</i> model</b>
5S rRNA	<i>Hm</i> 5S rRNA	3CC2.9	1-122	9
23S rRNA	<i>Hm</i> 23S rRNA	3CC2.0	10-2914 <sup>a</sup>	0
ES3	<i>Tt</i> 5.8S rRNA	4A17.2	115-134	8
ES5	<i>Tt</i> 26S rRNA	4A19.1	125-144	8
ES20	<i>Tt</i> 26S rRNA	4A19.1	1645-1678	8
ES24	<i>Sc</i> 25S rRNA	3O58.1	1753-1772	8
ES26	<i>Tt</i> 26S rRNA	4A19.1	1827-1849	8
ES41	<i>Tt</i> 26S rRNA	4A19.1	3302-3317	8

<sup>a</sup> Contains gaps to accommodate the insertions of expansion segments ES3, ES5, ES20, ES24, ES26, and ES41.

## Supplementary References

1. Menne, T. F., Goyenechea, B., Sánchez-Puig, N., Wong, C. C., Tonkin, L. M., Ancliff, P. J., Brost, R. L., Costanzo, M., Boone, C. & Warren, A. J. (2007). The Shwachman-Bodian-Diamond syndrome protein mediates translational activation of ribosomes in yeast. *Nat Genet* **39**, 486-95.
2. Lecompte, O., Ripp, R., Thierry, J.-C., Moras, D. & Poch, O. (2002). Comparative analysis of ribosomal proteins in complete genomes: an example of reductive evolution at the domain scale. *Nucleic Acids Research* **30**, 5382-90.
3. Cole, S. T., Eiglmeier, K., Parkhill, J., James, K. D., Thomson, N. R., Wheeler, P. R., Honoré, N., Garnier, T., Churcher, C., Harris, D., Mungall, K., Basham, D., Brown, D., Chillingworth, T., Connor, R., Davies, R. M., Devlin, K., Duthoy, S., Feltwell, T., Fraser, A., Hamlin, N., Holroyd, S., Hornsby, T., Jagels, K., Lacroix, C., Maclean, J., Moule, S., Murphy, L., Oliver, K., Quail, M. A., Rajandream, M. A., Rutherford, K. M., Rutter, S., Seeger, K., Simon, S., Simmonds, M., Skelton, J., Squares, R., Squares, S., Stevens, K., Taylor, K., Whitehead, S., Woodward, J. R. & Barrell, B. G. (2001). Massive gene decay in the leprosy bacillus. *Nature* **409**, 1007-11.
4. Katinka, M. D., Duprat, S., Cornillot, E., Méténier, G., Thomarat, F., Prensier, G., Barbe, V., Peyretailleade, E., Brottier, P., Wincker, P., Delbac, F., El Alaoui, H., Peyret, P., Saurin, W., Gouy, M., Weissenbach, J. & Vivarès, C. P. (2001). Genome sequence and gene compaction of the eukaryote parasite *Encephalitozoon cuniculi*. *Nature* **414**, 450-3.
5. Hershberg, R., Tang, H. & Petrov, D. A. (2007). Reduced selection leads to accelerated gene loss in *Shigella*. *Genome Biol* **8**, R164.
6. Andersson, S. G., Zomorodipour, A., Andersson, J. O., Sicheritz-Pontén, T., Alsmark, U. C., Podowski, R. M., Näslund, A. K., Eriksson, A. S., Winkler, H. H. & Kurland, C. G. (1998). The genome sequence of *Rickettsia prowazekii* and the origin of mitochondria. *Nature* **396**, 133-40.
7. Moran, N. A., McLaughlin, H. J. & Sorek, R. (2009). The dynamics and time scale of ongoing genomic erosion in symbiotic bacteria. *Science* **323**, 379-82.
8. Waters, E., Hohn, M. J., Ahel, I., Graham, D. E., Adams, M. D., Barnstead, M., Beeson, K. Y., Bibbs, L., Bolanos, R., Keller, M., Kretz, K., Lin, X., Mathur, E., Ni, J., Podar, M., Richardson, T., Sutton, G. G., Simon, M., Soll, D., Stetter, K. O., Short, J. M. & Noordewier, M. (2003). The genome of *Nanoarchaeum equitans*: insights into early archaeal evolution and derived parasitism. *Proc Natl Acad Sci USA* **100**, 12984-8.
9. Rocap, G., Larimer, F. W., Lamerdin, J., Malfatti, S., Chain, P., Ahlgren, N. A., Arellano, A., Coleman, M., Hauser, L., Hess, W. R., Johnson, Z. I., Land, M., Lindell, D., Post, A. F., Regala, W., Shah, M., Shaw, S. L., Steglich, C., Sullivan, M. B., Ting, C. S., Tolonen, A., Webb, E. A., Zinser, E. R. & Chisholm, S. W. (2003). Genome divergence in two *Prochlorococcus* ecotypes reflects oceanic niche differentiation. *Nature* **424**, 1042-7.
10. Dufresne, A., Garczarek, L. & Partensky, F. (2005). Accelerated evolution associated with genome reduction in a free-living prokaryote. *Genome Biol* **6**, R14.
11. Smole, Z., Nikolic, N., Supek, F., Šmuc, T., Sbalzarini, I. F. & Krisko, A. (2011). Proteome sequence features carry signatures of the environmental niche of prokaryotes. *BMC Evol Biol* **11**, 26.
12. Kennedy, S. P., Ng, W. V., Salzberg, S. L., Hood, L. & DasSarma, S. (2001). Understanding the adaptation of *Halobacterium* species NRC-1 to its extreme environment through computational analysis of its genome sequence. *Genome Research* **11**, 1641-50.

13. Gadbhir, M., Rasched, I., Marlière, P. & Mutzel, R. (1995). Convergent evolution of amino acid usage in archaeabacterial and eubacterial lineages adapted to high salt. *Res Microbiol* **146**, 113-20.
14. Rosenthal, P. B. & Henderson, R. (2003). Optimal determination of particle orientation, absolute hand, and contrast loss in single-particle electron cryomicroscopy. In *Journal of Molecular Biology*, Vol. 333, pp. 721-45.
15. Basu, U., Si, K., Deng, H. & Maitra, U. (2003). Phosphorylation of mammalian eukaryotic translation initiation factor 6 and its *Saccharomyces cerevisiae* homologue Tif6p: evidence that phosphorylation of Tif6p regulates its nucleocytoplasmic distribution and is required for yeast cell growth. *Mol Cell Biol* **23**, 6187-99.
16. Biswas, A., Mukherjee, S., Das, S., Shields, D., Chow, C. W. & Maitra, U. (2011). Opposing action of casein kinase 1 and calcineurin in nucleo-cytoplasmic shuttling of mammalian translation initiation factor eIF6. *J Biol Chem* **286**, 3129-38.
17. Ceci, M., Gaviraghi, C., Gorrini, C., Sala, L. A., Offenhäuser, N., Marchisio, P. C. & Biffo, S. (2003). Release of eIF6 (p27BBP) from the 60S subunit allows 80S ribosome assembly. *Nature* **426**, 579-84.
18. Finch, A. J., Hilcenko, C., Basse, N., Drynan, L. F., Goyenechea, B., Menne, T. F., González Fernández, A., Simpson, P., D'Santos, C. S., Arends, M. J., Donadieu, J., Bellanné-Chantelot, C., Costanzo, M., Boone, C., McKenzie, A. N., Freund, S. M. V. & Warren, A. J. (2011). Uncoupling of GTP hydrolysis from eIF6 release on the ribosome causes Shwachman-Diamond syndrome. *Genes & Development* **25**, 917-29.
19. Groft, C. M., Beckmann, R., Sali, A. & Burley, S. K. (2000). Crystal structures of ribosome anti-association factor IF6. *Nat Struct Biol* **7**, 1156-64.
20. Cannone, J. J., Subramanian, S., Schnare, M. N., Collett, J. R., D'Souza, L. M., Du, Y., Feng, B., Lin, N., Madabusi, L. V., Müller, K. M., Pande, N., Shang, Z., Yu, N. & Gutell, R. R. (2002). The comparative RNA web (CRW) site: an online database of comparative sequence and structure information for ribosomal, intron, and other RNAs. *BMC Bioinformatics* **3**, 2.
21. Klinge, S., Voigts-Hoffmann, F., Leibundgut, M. A., Arpagaus, S. & Ban, N. (2011). Crystal Structure of the Eukaryotic 60S Ribosomal Subunit in Complex with Initiation Factor 6. *Science* **334**, 941-8.
22. Thompson, J. D., Gibson, T. J. & Higgins, D. G. (2002). Multiple sequence alignment using ClustalW and ClustalX. *Curr Protoc Bioinformatics Chapter 2*, Unit 2.3.
23. Pettersen, E. F., Goddard, T. D., Huang, C. C., Couch, G. S., Greenblatt, D. M., Meng, E. C. & Ferrin, T. E. (2004). UCSF Chimera--a visualization system for exploratory research and analysis. *J Comput Chem* **25**, 1605-12.
24. Waterhouse, A. M., Procter, J. B., Martin, D. M. A., Clamp, M. & Barton, G. J. (2009). Jalview Version 2--a multiple sequence alignment editor and analysis workbench. *Bioinformatics* **25**, 1189-91.
25. UniProt Consortium. (2011). Ongoing and future developments at the Universal Protein Resource. *Nucleic Acids Research* **39**, D214-9.
26. Blaha, G., Gürel, G., Schroeder, S. J., Moore, P. B. & Steitz, T. A. (2008). Mutations outside the anisomycin-binding site can make ribosomes drug-resistant. In *Journal of Molecular Biology*, Vol. 379, pp. 505-19.
27. Ben-Shem, A., Jenner, L., Yusupova, G. & Yusupov, M. (2010). Crystal structure of the eukaryotic ribosome. *Science* **330**, 1203-9.